Generation of tunable entanglement and violation of a Bell-like inequality between different degrees of freedom of a single photon

Adam Vallés,[1,*] Vincenzo D'Ambrosio,[2] Martin Hendrych,[1] Michal Mičuda,[3] Lorenzo Marrucci,[4] Fabio Sciarrino,[2] and Juan P. Torres[1,5]

[1]*ICFO—Institut de Ciències Fotòniques, Mediterranean Technology Park, 08860, Castelldefels, Barcelona, Spain*

[2]*Dipartimento di Fisica, Sapienza Universita di Roma, Roma 00185, Italy*

[3]*Department of Optics, Palacký University, 17 listopadu 12, 77146 Olomouc, Czech Republic*

[4]*Dipartimento di Fisica, Universita di Napoli Federico II, Complesso Universitario di Monte Sant'Angelo, Napoli, Italy*

[5]*Department of Signal Theory and Communications, Universitat Politècnica de Catalunya, Jordi Girona 1-3, Campus Nord D3, 08034 Barcelona, Spain*

(Received 1 July 2014; published 20 November 2014)

We demonstrate a scheme to generate noncoherent and coherent correlations, i.e., a tunable degree of entanglement, between degrees of freedom of a single photon. Its nature is analogous to the tuning of the purity (first-order coherence) of a single photon forming part of a two-photon state by tailoring the correlations between the paired photons. Therefore, well-known tools such as the Clauser-Horne-Shimony-Holt (CHSH) Bell-like inequality can also be used to characterize entanglement between degrees of freedom. More specifically, CHSH inequality tests are performed, making use of the polarization and the spatial shape of a single photon. The four modes required are two polarization modes and two spatial modes with different orbital angular momentum.

DOI: 10.1103/PhysRevA.90.052326 PACS number(s): 03.67.Bg, 42.50.Dv, 42.50.Tx

I. INTRODUCTION

Entanglement, a concept introduced in quantum theory nearly eighty years ago by Schrödinger [1], is one of the main traits of quantum theory; for some it is even its weirdest feature [2]. Since the publication of the seminal gedanken experiment by Einstein, Podoslky, and Rosen (EPR) in their famous 1935 paper [3] and the appearance of the first comments about it the very same year [4], innumerable theoretical discussions and experiments related to this subject have appeared.

Arguably the most relevant contribution to this discussion has been the introduction, now fifty years ago, of the now well-known Bell inequalities [5]. One of these Bell-like inequalities, the Clauser-Horne-Shimony-Holt (CHSH) inequality [6], which will be used in this work, is the most commonly used one in experiments [7]. Originally, Bell's inequalities were considered for composite systems made up of two separate subsystems, i.e., two subsystems propagating along different directions that had interacted in the past.

For instance, the two subsystems can be each one of the two photons generated by means of the nonlinear process of spontaneous parametric down-conversion (SPDC), when an intense pump beam interacts with the atoms of a noncentrosymmetric nonlinear crystal [8]. Entanglement can reside in any of the degrees of freedom that characterize each of the photons, with being polarization the most common. In this case, one of the quantum states that allows a maximum violation of the CHSH inequality can be written as $|\Phi\rangle = 1/\sqrt{2}\,[a^{\dagger}_{k_1,H}a^{\dagger}_{k_2,V} + a^{\dagger}_{k_1,V}a^{\dagger}_{k_2,H}]|\text{vac}\rangle$, where $a^{\dagger}_{k_i,H}$ designates the creation operator of a photon propagating along direction k_i ($i = 1,2$) with polarization H, similarly for $a^{\dagger}_{k_i,V}$, and $|\text{vac}\rangle$ is the vacuum state.

However, correlations of a nature similar to the ones existing between physically separated photons can also exist considering different degrees of freedom of a single system. Therefore, Bell's inequalities can be used as well to characterize these correlations existing between different parts of a single system. The key point to consider regarding Bell's inequalities in this scenario is the capability to perform independent measurements in any of the degrees of freedom involved. In Ref. [9], a single photon was generated in the quantum state $|\Phi\rangle = 1/\sqrt{2}\,[a^{\dagger}_{k_1,H} + a^{\dagger}_{k_2,V}]|\text{vac}\rangle$, which violates a Bell-like inequality involving two degrees of freedom (polarization and path).

Bell-like inequalities can be also used to characterize beams containing many photons, i.e., intense beams, coherent or not. In Refs. [10,11], the authors make use of coherent beams whose electric field reads $\mathbf{E}(\mathbf{r}) = 1/\sqrt{2}\,[\Psi_H(\mathbf{r})\hat{\mathbf{e}}_H + \Psi_V(\mathbf{r})\hat{\mathbf{e}}_V]$ and use a CHSH inequality to characterize their coherence properties in one of the two degrees of freedom involved, i.e., polarization or the spatial shape. Entanglement, as the inseparability of degrees of freedom, has also been considered [12,13] as a fundamental tool to address and shed new light on certain characteristics of classical fields, by applying analysis and techniques usually restricted to entanglement in a quantum scenario.

Here we intend to move further into this analogy and show experimentally that one can generate tunable entanglement between two degrees of freedom of a single photon, going from the generation of coherent correlations to incoherent ones. For the single-photon case, the control of the degree of entanglement between degrees of freedom is fully equivalent to tuning the first-order coherence [14] of one of the degrees of freedom involved, in full analogy with the relationship existing between the degree of entanglement between separate photons and the first-order coherence of one of the photons that forms the pair.

Different types of quantum states provide different results in the measurement of the CHSH inequality. This

*adam.valles@icfo.es

notwithstanding, for any quantum state with any degree of first-order coherence or purity, we demonstrate that the results of a Bell's measurement obtained using different degrees of freedom of a single photon are the same as when using the properties of separate photons.

In our experiments we make use of single photons where the two degrees of freedom involved are the polarization (horizontal and vertical linear polarizations) and spatial modes (two spatial modes with orbital angular momentum index $m = \pm 1$). The orbital angular momentum (OAM) states allow for a relatively simple experimental generation, filtering, detection, and control [15]. These states are characterized by the index m, which can take any integer number, and determines the azimuthal phase dependence of the mode, which is of the form $\sim \exp(im\varphi)$. Each mode carries an OAM of $m\hbar$ per photon. The feasibility to generate entangled states in the laboratory using polarization and spatial modes with OAM is greatly facilitated by the use of the so-called q plates [16]: Liquid crystal devices which couple together polarization and orbital angular momentum and allow the generation of states that have been recently exploited in fundamental quantum mechanics [17,18], quantum communications [19], and metrology [20]. In Ref. [21], Nagali *et al.* generated a single-photon quantum state with the OAM and polarization degrees of freedom with high purity. Karimi *et al.* [22] used this same state to demonstrate the violation of the CHSH inequality.

II. EXPERIMENTAL SETUP

The experimental setup used in our experiments is shown in Fig. 1. Paired photons are generated in a 2-mm-long β-barium borate (BBO) nonlinear crystal by means of spontaneous parametric down-conversion (SPDC). We choose a type-II source, where the photons generated have orthogonal (horizontal and vertical) polarizations in order to generate a polarization-entangled photon pair by postselection with a beam splitter and a coincidence detection.

The pumping laser is a Mira 900 (Coherent) working in the picosecond regime and tuned to a central wavelength of 810 nm. In order to obtain the down-converted photons at 810 nm, light from Mira is frequency doubled in a second-harmonic setup (Inspire Blue, Radiantis). The output light at 405 nm traverses an optical system with five dichroic mirrors and a short-pass filter to filter out the remaining 810-nm light. A spatial filter tailors the spatial shape of the pump beam to obtain the sought-after Gaussian beam profile. We use a 750-mm focal distance lens to obtain a pump beam with 400-μm beam waist that is focused in the middle of the nonlinear crystal. A smaller beam waist would increase efficiency of the SPDC process; however, the spatial walkoff in the BBO crystal impedes tighter focusing, because it would also introduce harmful spatial distinguishability between the generated photons. The down-converted photons are collimated with a 400-mm focal distance lens.

Another filtering system, formed by two dichroic mirrors, a long-pass filter, and a band-pass filter, removes the residual pump light at 405 nm. Different group velocities result in slightly different spectra of the orthogonal polarizations, thus mixing the polarization and frequency properties of the photons. The use of a filter with 3-nm full-width-half-maximum bandwidth centered at 810 nm helps reducing the spectral distinguishability between the photons.

After the beam splitter, the quantum state of the two photons, considering only the cases when the paired photons are detected in coincidence (postselection), can be generally written as

$$\rho = \epsilon|\Psi\rangle\langle\Psi| + \frac{1-\epsilon}{2} \times \{|H\rangle_1|V\rangle_2\langle H|_1\langle V|_2 + |V\rangle_1|H\rangle_2\langle V|_1\langle H|_2\}, \quad (1)$$

where indexes 1 and 2 refers to paths 1 and 2 after the beam splitter, $|\Psi\rangle = 1/\sqrt{2}\,[|H\rangle_1|V\rangle_2 + |V\rangle_1|H\rangle_2]$, and ϵ depends on the delay (τ) between the two orthogonal photons generated. The form of the state given by Eq. (1) is due to the correlation exiting between the polarization of the photon generated and its group velocity, since the nonlinear crystal used (BBO) is a birefringent crystal. In particular, the group velocity of photons at 810 nm with horizontal polarization (ordinary wave) is $v_g^o = 1.7816\times10^8$ m/s, while the group velocity of photons with vertical polarization (extraordinary wave) is $v_g^e = 1.8439\times10^8$ m/s, which produces a group velocity mismatch (GVM) of $D_{\mathrm{BBO}} = 1/v_g^o - 1/v_g^e = 189.6$ fs/mm. This distinguishability of photons by its group velocity cause the mixed character of the quantum state in polarization given by Eq. (1).

A delay line, formed by quartz prisms, can be used to tune its value. If photons could be distinguished by their time of arrival at the detectors, then $\epsilon = 0$ and the purity of the quantum state that describes the two photons generated is minimal ($P = 1/2$). The purity of the quantum state can be increased by adding or removing the length of quartz that the photons traverse along its optical path [23], which is necessary to remove all distinguishing information coming from the temporal-frequency degree of freedom. The group velocity of ordinary waves in quartz is $v_g^o = 1.9305\times10^8$ m/s, while the group velocity of extraordinary waves is $v_g^e = 1.9187\times10^8$, which produces a GVM of $D_{\mathrm{quartz}} = -31.8$ fs/mm. For a specific arrangement of the quartz prisms, that we define as $\tau = 0$, we can have $\epsilon = 1$. For the $L = 2$ mm long BBO crystal of our experiment, with group velocity mismatch of $D_{\mathrm{BBO}} = 189.6$ fs/mm, this requires [24] compensating with the tunable delay line $D_{\mathrm{BBO}}L/2 = 189.6/2$ fs/mm$\times$2 mm $=$ 189.6 fs.

To entangle the polarization and the orbital angular momentum (OAM) degrees of freedom in a single photon, the photon reflected from the the beam splitter (photon 1) is projected into the linear diagonal polarization state $1/\sqrt{2}\,[|H\rangle \pm |V\rangle]$, with a half-wave plate (HWP_1) and a Glan-Thompson polarizer (GT_1), coupled into a single mode fiber, to remove the remaining spatial distinguishability introduced by the presence of spatial walkoff in the BBO crystal and detect it in coincidences (coincidence time window of 12.5 ns). The transmitted photon (photon 2) traverses a quarter-wave plate (QWP_1) to rotate its polarization from horizontal and vertical to circular right (**R**) and circular left (**L**), a q plate (QP_1) correlates polarization with OAM, and another quarter-wave plate (QWP_2) transforms the polarization back from circular right and circular left to

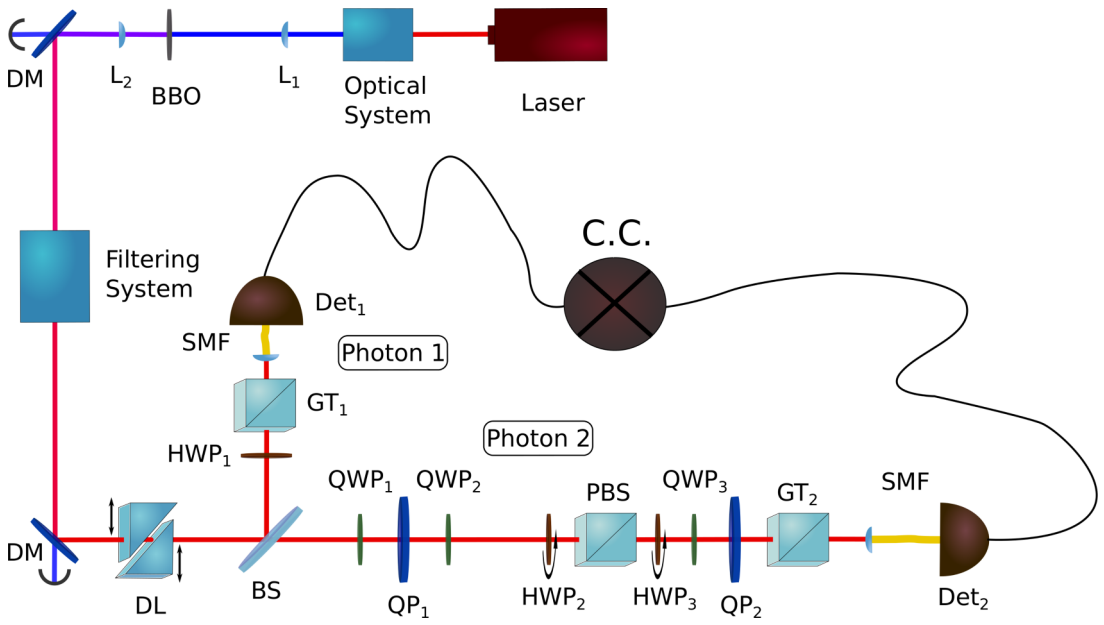

FIG. 1. (Color online) Experimental setup scheme. Laser: Mira 900 (Coherent). Optical system: second harmonic generation (Inspire Blue, Radiantis), spatial filter, linear attenuator, three dichroic mirrors (DM), and short pass filter. L_1 and L_2: Fourier lenses. BBO: nonlinear crystal. Filtering system: long-pass and band-pass filters. DL: delay line. BS: beam splitter (50:50). HWP_1, HWP_2, and HWP_3: half-wave plates. PBS: polarization beam splitter. GT_1 and GT_2: Glan-Thompson polarizers. QWP_1, QWP_2, and QWP_3: quarter-wave plates. QP_1 and QP_2: q plates. Det_1 and Det_2: single-photon counting modules. C.C.: coincidence-counting electronics.

horizontal and vertical. In summary,

$$|\mathbf{H}\rangle \Rightarrow |\mathbf{R}\rangle \Rightarrow |\mathbf{L},\mathbf{m}=-\mathbf{1}\rangle \Rightarrow |\mathbf{H},\mathbf{m}=-\mathbf{1}\rangle,$$
$$|\mathbf{V}\rangle \Rightarrow |\mathbf{L}\rangle \Rightarrow |\mathbf{R},\mathbf{m}=+\mathbf{1}\rangle \Rightarrow |\mathbf{V},\mathbf{m}=+\mathbf{1}\rangle. \quad (2)$$

After the second quarter-wave plate, the quantum state of photon 2, after projection and detection of photon 1, is written as

$$\rho = \epsilon|\Psi^{\pm}\rangle\langle\Psi^{\pm}| + \frac{1-\epsilon}{2}[|H,m=-1\rangle\langle H,m=-1| + |V,m=+1\rangle\langle V,m=+1|], \quad (3)$$

where

$$|\Psi^{\pm}\rangle\frac{1}{\sqrt{2}}(|H,m=-1\rangle \pm |V,m=+1\rangle). \quad (4)$$

The purity of the state is $P=(1+\epsilon^2)/2$. If one would apply the concept of concurrence [25] to this single-photon state, considering as the two subsystems the polarization and OAM degrees of freedom of the photon, one would obtain $C=\epsilon$.

The measurement stage consist of projecting the quantum state generated into specific polarization and OAM states in two steps. First, the state of polarization is projected into the desired state with a half-wave plate (HWP_2) and a polarizing beam splitter (PBS). The OAM can be projected into any state using several polarization optic elements, before and after a second q plate (QP_2) [21]. More specifically, the OAM state information is transferred into a polarization state with a half-wave plate (HWP_3) and a quarter-wave plate (QWP_3) located before the q plate, to transform horizontal-vertical polarizations to right-left polarizations base, and another Glan-Thompson polarizer (GT_2) located after. Finally, the photon is spatially filtered by coupling it to a single-mode fiber and detecting it in coincidence with the other photon.

III. EXPERIMENTAL RESULTS

In order to be able to relate the value of ϵ in Eq. (3) to the delay introduced by the delay line and determine the value of the delay which makes the quantum state pure ($\epsilon=1$), we construct a Hong-Ou-Mandel interferometer (HOM). If we choose the temporal delay introduced by the delay line so that coincidences are close to zero, the state given by Eq. (3) is pure ($\epsilon=1$) and corresponds to a Bell state. We choose to generate the quantum state $|\Psi^-\rangle$ to obtain the HOM dip. Figure 2(a) shows the coincidence photons measured in detectors 1 and 2, and Fig. 2(b) shows the single photons detected in each detector. Figure 2(c) shows coincidence detections renormalized using the single measurements from detector 1. The oscillations in detector 1 are due to imperfections in the translation stage of the delay line (DL), causing deviations in the photon trajectories. Thus the single detections of detector 1 are clearly affected by these corresponding variations in the coupling efficiency. We should notice that all the results presented in this paper are shown with no substraction of the accidental coincidences (~4 pairs in 10 s).

When we change the projection of photon 1 from the state $1/\sqrt{2}\,[|H\rangle + |V\rangle]$ to $1/\sqrt{2}\,[|H\rangle - |V\rangle]$ with HWP_1, we change the sign of the corresponding Bell state from $|\Psi^-\rangle$ to $|\Psi^+\rangle$. By modifying the transformation of photon 2 from $L/R \Rightarrow H/V$ to $L/R \Rightarrow V/H$ with QWP_2, we can go from the generation of $|\Psi^{\pm}\rangle$ to $|\Phi^{\pm}\rangle$, where $\Phi^{\pm}$ can be written as

$$|\Phi^{\pm}\rangle = \frac{1}{\sqrt{2}}(|H,m=+1\rangle \pm |V,m=-1\rangle). \quad (5)$$

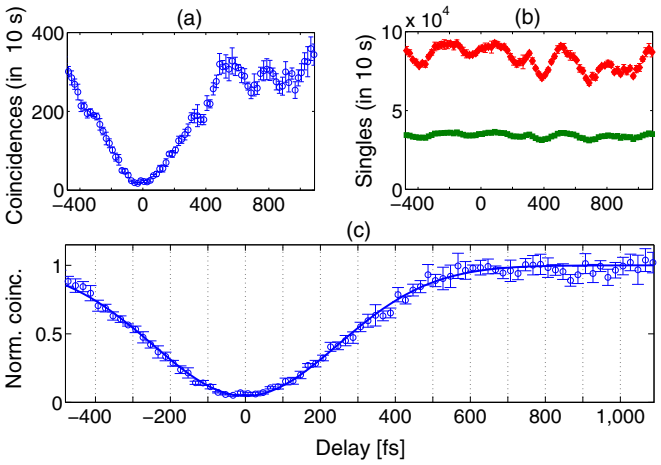

FIG. 2. (Color online) Coincidence and singles detections as a function of the temporal delay τ in a Hong-Ou-Mandel (HOM) interferometer. The raw data of the coincidences measured in 10 s are plotted in panel (a), and the singles detected for each detector are shown in panel (b). Closed diamonds (upper curve) correspond to singles detected with detector 1, and closed squares (lower curve) correspond to measurements in detector 2. The compensated and normalized number of coincidences is plotted in panel (c), using the coincidence data of panel (a) and the singles detected with detector 1 shown in panel (b).

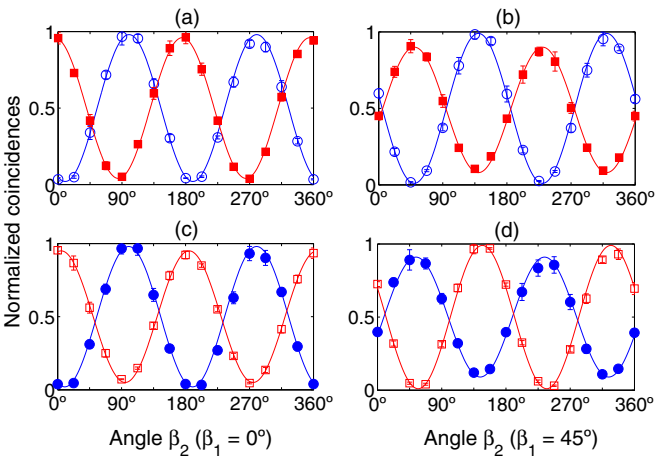

FIG. 3. (Color online) Normalized value of the coincidences as a function of the projection angle β_2. Panels (a) and (c): the angle of HWP_2 is set to $\beta_1 = 0°$; panels (b) and (d): the angle is set to $\beta_1 = 45°$. Curves corresponding to experimental values are shown with error bars. Solid lines are theoretical predictions. Open circles, $|\Psi^-\rangle$; closed circles, $|\Psi^+\rangle$; open squares, $|\Phi^-\rangle$; and closed squares, $|\Phi^+\rangle$.

With this procedure we are able to create the four Bell states.

Figure 3 shows the coincidences measured for each of the four Bell states. Photon 2 is projected first into the polarization state $\sim\cos\beta_1\,|H\rangle + \sin\beta_1\,|V\rangle$, with $\beta_1 = 0°,45°$, and after that a second projection is performed into a set of OAM states of the form $\cos\beta_2\,|+1\rangle + \sin\beta_2\,|-1\rangle$, with β_2 spanning from 0 to 2π. Ideally, for the state $|\Psi^-\rangle$, coincidence counts as a function of β_2 follow the form of $\sin^2(\beta_1 - \beta_2)$, which yields a visibility [24] $V = (\max - \min)/(\max + \min)$ of 100%. Therefore, as the visibility measured increased, so did the quality of the entangled state generated. The small phase shifts observed in the curves are due to some misalignment still present between the position of the centers of the vortex of the two OAM modes, $m = +1$ and $m = -1$, when going through the second q plate (QP_2).

Measurements of the CHSH inequality [6] require choosing two polarization states and two OAM states where the state of photon 2, given by Eq. (3), is projected. When considering any possible state projection, following Ref. [26], one finds that the maximum violation of the CHSH inequality for this state is

$$S_{\max} = 2\sqrt{1+\epsilon^2}. \tag{6}$$

For $\epsilon = 1$ we reach the Tsirelson bound. We will restrict the discussion here to only projections into states of the form

$$|\mathbf{a}_i\rangle = \frac{1}{\sqrt{2}}\left(\cos a_i\,|H\rangle + \sin a_i\,|V\rangle\right),$$
$$|\mathbf{b}_i\rangle = \frac{1}{\sqrt{2}}\left(\cos b_i\,|m=+1\rangle + \sin b_i\,|m=-1\rangle\right), \tag{7}$$

where states $\mathbf{a}_i$ $(i = 1,2)$ refer to linear polarization states and $\mathbf{b}_i$ $(i = 1,2)$ refer to OAM states, which are linear combinations of modes $m = +1$ and $m = -1$. By proper combinations of all of the polarization optical elements of the setup (half-wave and quarter-wave plates), one can project the photon into any combination $(\mathbf{a}_i, \mathbf{b}_i)$ as required.

For the single-photon case, restricting our attention to state projections of the form given in Eq. (7), the CHSH inequality can be written as

$$S = E(a_1,b_1) - E(a_1,b_2) + E(a_2,b_1) + E(a_2+b_2) \leqslant 2, \tag{8}$$

where

$$E(a_i,b_i) = \frac{N_{++}(a_i,b_i) + N_{--}(a_i^\perp,b_i^\perp) - N_{+-}(a_i,b_i^\perp) - N_{-+}(a_i^\perp,b_i)}{N_{++}(a_i,b_i) + N_{--}(a_i^\perp,b_i^\perp) + N_{+-}(a_i,b_i^\perp) + N_{-+}(a_i^\perp,b_i)}. \tag{9}$$

$N_{++}(a_i,b_i)$ is the number of photons detected when its quantum state is projected into a polarization state determined by the angle a_i and an OAM state determined by the angle b_i. All other cases follow similarly, taking into account that $a_i^\perp = a_i + \pi/2$ and $b_i^\perp = b_i + \pi/2$. One can easily find that for the state given by Eq. (3),

$$E(a_i,b_i) = \cos 2a_i \cos 2b_i + \epsilon \sin 2a_i \sin 2b_i. \tag{10}$$

Figure 4 shows the value of S measured when we go from a pure to a mixed state, i.e., for different values of ϵ from 0 to 1.

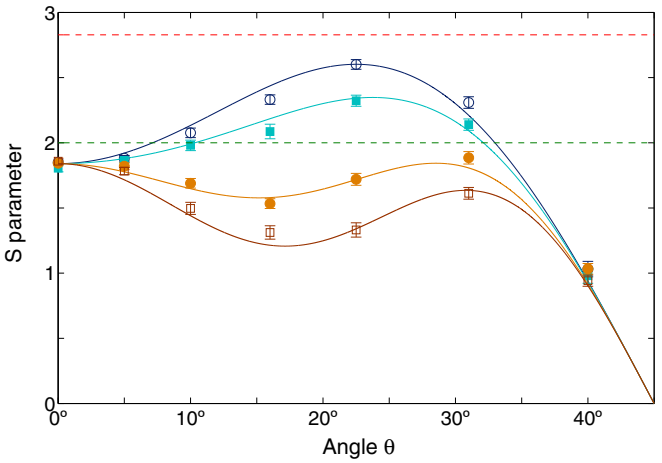

FIG. 4. (Color online) Value of the parameter S in a CHSH inequality as a function of the angle $\theta = b_1 - a_1$. The colored symbols with error bars represent the experimental data with their standard deviations. The solid colored curves are the theoretical predictions assuming a visibility factor of $V = 0.92$. Open circles, $\epsilon = 1$; closed squares, $\epsilon = 0.8$; closed circles, $\epsilon = 0.32$; and open squares, $\epsilon = 0.03$. The values of ϵ correspond to delays of 0 fs ($\epsilon = 1$), 200 fs ($\epsilon = 0.8$), 400 fs ($\epsilon = 0.32$), and 600 fs ($\epsilon = 0.03$), as depicted in the HOM dip of Fig. 2. The dashed red line (upper) corresponds to the Tsirelson bound, and the dashed green line (lower) is the CHSH inequality limit.

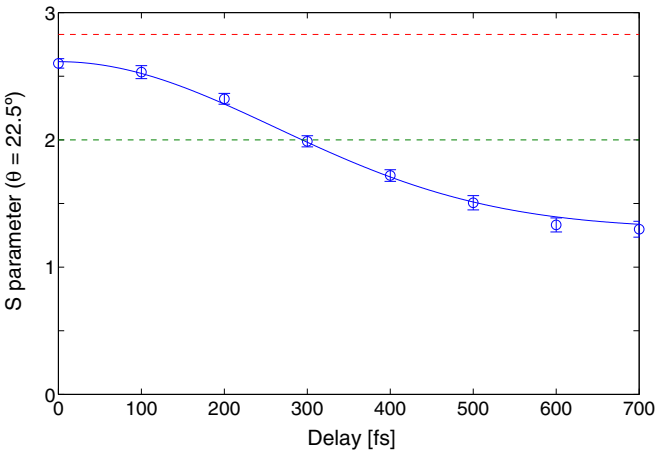

FIG. 5. (Color online) Value of the CHSH inequality for $\theta = 22.5^\circ$ as a function of the temporal delay, as depicted in Fig. 2. The solid (blue) curve is the theoretical prediction assuming a visibility factor of $V = 0.92$. The dashed red line (upper) corresponds to the Tsirelson bound ($S_{\max} = 2\sqrt{2}$), and the dashed green line (lower) is the CHSH inequality limit ($S = 2$).

It shows the value of S as a function of the angle θ, where $\theta \equiv b_1 - a_1 = b_2 + a_2 = -b_1 - a_2$. For the case of a pure state, one would obtain $S(\theta) = 3\cos 2\theta - \cos 6\theta$. The experimental values measured decrease from the theoretical (ideal) expected values due to the existence of accidental coincidences or the inevitable misalignment of optical elements, by a factor V, the visibility measured in Fig. 3. In our case, the maximum CHSH inequality value measured is $S(\theta = 22.5^\circ) = 2.601 \pm 0.037$ and the visibility is $V = 0.92$.

Figure 4 shows that there is a complete analogy between a Bell-like inequality involving the same degree of freedom of two separate photons [7,26] and that involving two distinct degrees of freedom of the same single photon, independent of the purity (or first-order coherence) of the quantum state. Figure 5 shows the CHSH violation measured for $\theta = 22.5^\circ$, which gives the maximum violation for a pure state. When the delay increases or decreases from τ_0, the state becomes increasingly mixed and entanglement disappears. Figures 4 and 5 are very similar to what would have been obtained for the case of two separate correlated photons, even though here the measurement corresponds to measuring correlations between properties in different degrees of freedom of a single photon. The similarities in form between the quantum states with different numbers of photons are why we obtain similar results, as it has been pointed out in several theoretical papers [12,13] and experiments [9,10].

IV. CONCLUSIONS

In conclusion, we have demonstrated experimentally that there is a full analogy between the general quantum state (pure or mixed) that describes two-photon states entangled in its polarization degree of freedom and the correlations (coherent or noncoherent) existing between the polarization and spatial degrees of freedom of a single photon. Along these lines, concepts such as purity and degree of entanglement or concurrence can be used to describe coherent and noncoherent correlations between properties of a single system. This fact naturally allows one to use Bell's inequalities to characterize both types of systems, as we have demonstrated here.

ACKNOWLEDGMENTS

We thank Fabrizio Bisesto for his collaboration in the first stage of the experiment. This work was supported by the project FIS2010-14831, the program Severo Ochoa from the Government of Spain, and the FET-Open Program, within the Seventh Framework Program of the European Commission under Grant No. 255914 (PHORBITECH). This work has also been partially supported by Fundacio Privada Cellex Barcelona. V.D'A. and F.S. acknowledge support via the Starting Grant 3D-QUEST (3D-Quantum Integrated Optical Simulation; Grant Agreement No. 307783). M.M. acknowledges support by the European Social Fund and MSMT under Project No. EE2.3.20.0060.

[1] E. Schrödinger, Math. Proc. Cambridge Philos. Soc. **31**, 555 (1935).
[2] S. Weinberg, *Lectures on Quantum Mechanics* (Cambridge University Press, New York, 2013).
[3] A. Einstein, B. Podolsky, and N. Rosen, Phys. Rev. **47**, 777 (1935).
[4] N. Bohr, Phys. Rev. **48**, 696 (1935).
[5] J. S. Bell, Physics (NY) **1**, 195 (1964).

[6] J. F. Clauser, M. A. Horne, A. Shimony, and R. A. Holt, Phys. Rev. Lett. **23**, 880 (1969).
[7] A. Aspect, J. Dalibard, and G. Roger, Phys. Rev. Lett. **49**, 1804 (1982).
[8] J. P. Torres, K. Banaszek, and I. A. Walmsley, Prog. Optics **56**, 227 (2011).
[9] B. R. Gadway, E. J. Galvez, and F. De Zela, J. Phys. B: At. Mol. Opt. Phys. **42**, 015503 (2009).
[10] C. V. S. Borges, M. Hor-Meyll, J. A. O. Huguenin, and A. Z. Khoury, Phys. Rev. A **82**, 033833 (2010).
[11] K. H. Kagalwala, G. Di Giuseppe, A. F. Abouraddy, and B. E. A. Saleh, Nat. Photon. **7**, 72 (2013).
[12] B. N. Simon, S. Simon, F. Gori, M. Santarsiero, R. Borghi, N. Mukunda, and R. Simon, Phys. Rev. Lett. **104**, 023901 (2010).
[13] X-F. Qian and J. H. Eberly, Opt. Lett. **36**, 4110 (2011).
[14] U. M. Titulaer and R. J. Glauber, Phys. Rev. **145**, 1041 (1966).
[15] G. Molina-Terriza, J. P. Torres, and L. Torner, Nat. Phys. **3**, 305 (2007).
[16] L. Marrucci, C. Manzo, and D. Paparo, Phys. Rev. Lett. **96**, 163905 (2006).
[17] E. Nagali, V. D'Ambrosio, F. Sciarrino, and A. Cabello, Phys. Rev. Lett. **108**, 090501 (2012).
[18] V. D'Ambrosio, I. Herbauts, E. Amselem, E. Nagali, M. Bourennane, F. Sciarrino, and A. Cabello, Phys. Rev. X **3**, 011012 (2013).
[19] V. D'Ambrosio, E. Nagali, S. P. Walborn, L. Aolita, S. Slussarenko, L. Marrucci, and F. Sciarrino, Nat. Commun. **3**, 961 (2012).
[20] V. D'Ambrosio, N. Spagnolo, L. Del Re, S. Slussarenko, Y. Li, L. C. Kwek, L. Marrucci, S. P. Walborn, L. Aolita, and F. Sciarrino, Nat. Commun. **4**, 2432 (2013).
[21] E. Nagali, F. Sciarrino, F. De Martini, L. Marrucci, B. Piccirillo, E. Karimi, and E. Santamato, Phys. Rev. Lett. **103**, 013601 (2009).
[22] E. Karimi, J. Leach, S. Slussarenko, B. Piccirillo, L. Marrucci, L. Chen, W. She, S. Franke-Arnold, M. J. Padgett, and E. Santamato, Phys. Rev. A **82**, 022115 (2010).
[23] M. Hendrych, R. Gallego, M. Mičuda, N. Brunner, A. Acín, and J. P. Torres, Nat. Phys. **8**, 588 (2012).
[24] P. G. Kwiat, K. Mattle, H. Weinfurter, A. Zeilinger, A. V. Sergienko, and Y. Shih, Phys. Rev. Lett. **75**, 4337 (1995).
[25] W. K. Wootters, Phys. Rev. Lett. **80**, 2245 (1998)
[26] R. Horodecki, P. Horodecki, and M. Horodecki, Phys. Lett. A **200**, 340 (1995).